Modeling and Control of VSI type FACTS controllers for Power System Dynamic Stability using the current injection method

Jungsoo Park, Gilsoo Jang*, and Kwang M. Son

Abstract: This paper describes modeling Voltage Sourced Inverter (VSI) type Flexible AC Transmission System (FACTS) controllers and control methods for power system dynamic stability studies. The considered FACTS controllers are the Static Compensator (STATCOM), the Static Synchronous Series Compensator (SSSC), and the Unified Power Flow Controller (UPFC). In this paper, these FACTS controllers are derived in the current injection model, and it is applied to the linear and nonlinear analysis algorithm for power system dynamics studies. The parameters of the FACTS controllers are set to damp the inter-area oscillations, and the supplementary damping controllers and its control schemes are proposed to increase damping abilities of the FACTS controllers. For these works, the linear analysis for each FACTS controller with or without damping controller is executed, and the dynamic characteristics of each FACTS controller are analyzed. The results are verified by the nonlinear analysis using the time-domain simulation.

Keywords: FACTS, FACTS control, power system dynamic stability, SSSC, STATCOM, UPFC.

1. INTRODUCTION

Flexible AC transmission system (FACTS) controllers are power electronics based devices. Among these power electronics controllers, the most advanced type is the controller that employs voltage sourced inverters (VSI) as synchronous voltage sources [1]. Representative VSI type FACTS controllers are the static compensator (STATCOM), which is a shunt type controller, the static synchronous series compensator (SSSC), which is a series type controller, and which is the unified power flow controller (UPFC), a combined series-shunt type controller [2].

The concepts and the performances of FACTS controllers are described in [3-5]. Subsequently, the studies for dynamic modeling and control methods have been conducted [6-8]. However, since the controllers have the nonlinear and complex characteristics, it is hard to model and analyze the power system in which FACTS controllers are installed. For that reason, most researches are focused on the modeling and the simulation of switch functions of FACTS controllers using EMTP, and current researches are interested in the steady-state analysis and the stability evaluation for FACTS installations [9,10].

In order to solve the difficulties, a unified model of series connected FACTS controllers is presented in [6]. The Jacobian of the power flow is modified to satisfy the node power relations for the node where the FACTS controllers are installed. Its modeling is based on the power equivalence at the FACTS node. In [7] and [8], a unified model of FACTS controllers, which uses the linearized Phillips-Heffron model for a power system, is proposed. The model is useful for control system design for various FACTS controllers. However, the methods are difficult to fit the algorithms into a conventional power system program.

In [11], the voltage that is injected by inverters of the UPFC and the energy exchange between the inverters are converted into the equivalent currents injected to the external nodes, and then they are solved by Newton iteration method similar to nonlinear loads in every time step. In this paper, the current injection model is adopted for studying dynamic stability of power system in which FACTS controllers are installed. All of VSI type FACTS controllers, which are STATCOM, SSSC, and UPFC, are considered, and the supplementary controller is

Manuscript received February 29, 2008; accepted May 28, 2008. Recommended by Guest Editor Seung Ki Sul. This work was supported by a Korea University grant, and by the Korea Science and Engineering Foundation (KOSEF) NRL Program grant funded by the Korea government (MEST) (No. R0A-2008-000-20107-0).

Jungsoo Park and Gilsoo Jang are with the School of Electrical Engineering, Korea University, 5-1 Anam-dong, Seongbuk-gu, Seoul 136-713, Korea (e-mails: {jspark98, gjang}@korea.ac.kr).

Kwang M. Son is with the department of Electrical Engineering, Dong-eui University, 995 Eomgwang-no, Busanjin-gu, Busan 614-714, Korea (e-mail: kmson@deu.ac.kr).

* Corresponding author.

designed to damp low-frequency inter-area oscillations. All parameters of FACTS controller and damping controller are set to increase the damping of inter-area oscillations using the linear analysis. The results are verified by time-domain simulations.

2. FACTS MODELING

The VSI type FACTS controller can internally generate both capacitive and inductive reactive power for transmission line compensation. The inverter, which is supported by a DC capacitor, can also exchange active power with the AC system in addition to the independently controllable reactive power [1]. The active power exchange can make the voltage fluctuation on DC capacitor during transient. However, the DC voltage perturbation is less than 1.5% of the rated voltage [12], and compared with the transient phenomena, the major frequency of power system dynamics is very low. Additionally, the considered oscillations in this paper have a low-frequency the range, within 0.1~2Hz. So, it is assumed that the DC capacitor voltage is stiff for the mentioned frequency range [11].

2.1. STATCOM

As shown in Fig. 1(a), the STATCOM has one inverter which is connected to the external node with a shunt transformer. E_{in} is the magnitude of voltage generated by the shunt inverter, and x_t is the impedance of shunt transformer.

The STATCOM supplies the reactive power to the external node for the voltage regulation. Thus, it is assumed that the inverter is the ideal voltage source having the same phase angle with the external node. The reactive power can be derived in the equivalent current source, $\mathbf{I_Q}$, having 90° phase angle difference with the external voltage, as shown in Fig. 1(b). It can be derived as follows,

$$\mathbf{I_Q} = I_Q \exp\, j\left(\theta^f - \frac{\pi}{2}\right) \tag{1}$$

$$I_Q = \frac{E_{in} - V^f}{x_t} \tag{2}$$

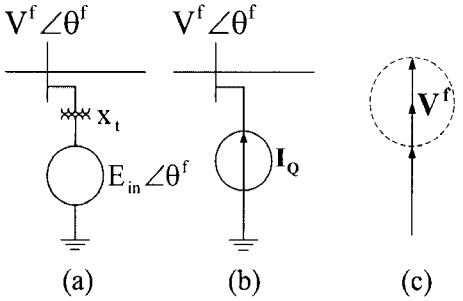

Fig. 1. (a) STATCOM model, (b) its equivalent current model, (c) the voltage phase diagram.

where the V^f and the θ^f indicate the voltage magnitude and the phase angle of the external node. The compensation effect on the external node voltage is illustrated in Fig. 1(c).

2.2. SSSC

The schematic representation of SSSC is shown in Fig. 2(a). The SSSC is composed of one inverter and a series transformer. Unlike the STATCOM, the transformer is connected in series with transmission line. It is assumed that the SSSC is an ideal reactive power source that generates voltage having the same phase with the voltage on the series transformer, x_S.

As shown in Fig. 2(c), the SSSC can control the voltage difference between the nodes 1 and 2. Consequently, it can regulate the phase angle difference between the voltages on the nodes 1 and 2, θ_{12}^f, in order to control the active power flow in transmission line. The phase angle, θ_q, of the series injected voltage, $\mathbf{V_q}$, is the same as the phase angle of voltage vector, $\mathbf{V_{12}^f}(=\mathbf{V_1^f} - \mathbf{V_2^f})$. It can be derived as follows,

$$\mathbf{V_q} = V_q \exp j\theta_q, \tag{3}$$

$$\theta_q = \tan^{-1}\frac{V_1^f \cos\theta_1^f - V_2^f \cos\theta_2^f}{V_1^f \sin\theta_1^f - V_2^f \sin\theta_2^f}, \tag{4}$$

where the subscripts 1 and 2 correspond to the nodes 1 and 2 in Fig. 2(a).

As described in equation (4), the injected voltage by SSSC depends on the external node voltages. The relation is implicit and nonlinear. To solve the complexities, the injected voltage, $\mathbf{V_q}$, is converted to a pair of the equivalent current sources, $\pm\mathbf{I_q}$, using

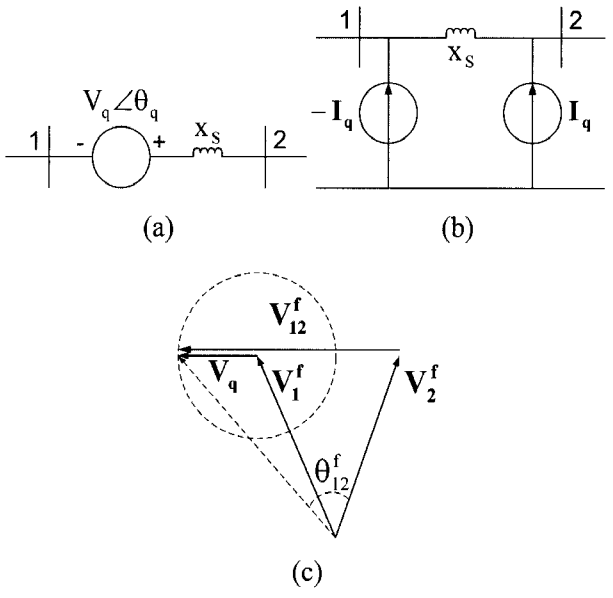

Fig. 2. (a) SSSC model, (b) its equivalent current model, (c) the voltage phase diagram.

Thevnin equivalent method as shown in Fig. 2(b). It can be derived as follows,

$$\mathbf{I_q} = \frac{\mathbf{V_q}}{jx_S} = \frac{V_q}{x_S}\exp j\left(\theta_q - \frac{\pi}{2}\right). \tag{5}$$

2.3. UPFC

The UPFC is the series-shunt combined type FACTS controller. As shown in the Fig. 3, it is composed of the series and the shunt inverters and the series and the shunt connected transformers. Therefore, it can be controlled the external node voltage and the active and reactive power flows in the transmission line. Unlike the other FACTS controllers, the series inverter of UPFC can inject the active power into the transmission line. The active power injected by series inverter is drawn, via DC capacitor, from the external node on the shunt inverter side.

The injected voltage, $\mathbf{V_S}$, by the series inverter is superimposed on the voltage of the shunt inverter side node, which is the node 1 in Fig. 3. Therefore, the resulting voltage can be derived as follows,

$$\mathbf{V_{S1}} = \mathbf{V_S}\exp j\theta_1^f = V_S\exp j\left(\theta_S + \theta_1^f\right). \tag{6}$$

where θ_1^f indicates the phase angle of the voltage on the shunt inverter side node, and the subscript S1 implies that the series injected voltage, $\mathbf{V_S}$, is superimposed on the shunt inverter side voltage, $\mathbf{V_1^f}$.

In [11], the series injected voltage by the UPFC is converted into a pair of Thevnin equivalent current sources, $\pm\mathbf{I_S}$. It can be derived as follows,

$$\mathbf{I_S} = \frac{\mathbf{V_{S1}}}{jx_S} = \frac{V_S}{x_S}\exp j\left(\theta_S + \theta_1^f - \frac{\pi}{2}\right). \tag{7}$$

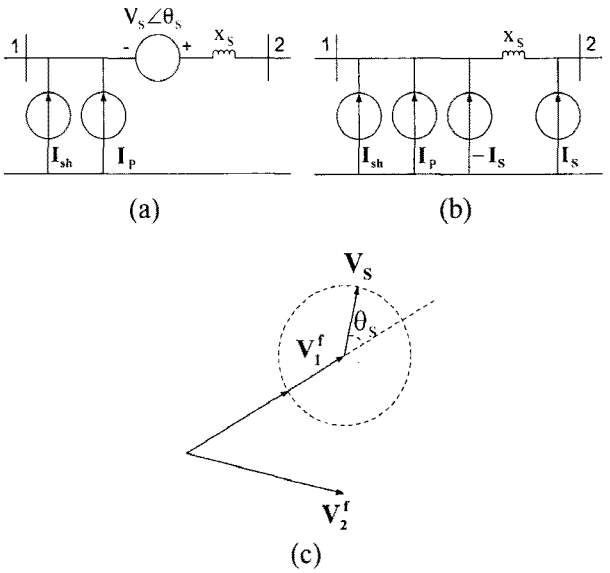

Fig. 3. (a) UPFC model, (b) its equivalent current model, (c) the voltage phase diagram.

Another current, $\mathbf{I_{sh}}$, on the shunt inverter side node is the injected current by the shunt inverter. It is the same current source as STATCOM in (1), with the exception of the subscript, sh.

$$\mathbf{I_{sh}} = I_{sh}\exp j\left(\theta^f - \frac{\pi}{2}\right). \tag{8}$$

The other current source, $\mathbf{I_P}$, is the equivalent current of the active power injected by the series inverter to the transmission line. The active power supplied by the series inverter can be calculated as follows,

$$P^f = \mathrm{Re}\left[\mathbf{V_2^f}\times\mathbf{I_S^*} - \mathbf{V_1^f}\times\mathbf{I_S^*}\right], \tag{9}$$

$$P^f = -\frac{V_1^f V_S}{x_S}\sin\theta_S + \frac{V_2^f V_S}{x_S}\sin\theta_S\cos\left(\theta_1^f - \theta_2^f\right) + \frac{V_2^f V_S}{x_S}\cos\theta_S\sin\left(\theta_1^f - \theta_2^f\right). \tag{10}$$

As mentioned above, the active power is drawn by the shunt inverter from the external circuit. Therefore, it can be derived as follows,

$$\mathbf{V_1^f}\times\mathbf{I_P^*} = -P^f, \tag{11}$$

$$\mathbf{I_P} = -\frac{P^f}{V_1^f}\exp j\theta_1^f. \tag{12}$$

3. POWER SYSTEM MODELING

The power system dynamic model can be written as a set of differential equations and a set of algebraic equations as follows,

$$\dot{\mathbf{x}} = \mathbf{f}(\mathbf{x},\mathbf{V}), \tag{13}$$

$$\mathbf{I}(\mathbf{x},\mathbf{V}) = \mathbf{YV}, \tag{14}$$

where $\mathbf{x}$ is a m dimensional state variable vector, and $\mathbf{I}$ and $\mathbf{V}$ are n dimensional complex injection currents and voltage vectors, respectively. The number m depends on the number and the type of the dynamic models, and the number n is equal to the number of buses in power system. The differential and the algebraic equations of each FACTS controller may be derived as follows.

3.1. Dynamic model

Fig. 4(a) shows the structure of the control system of the STATCOM and the shunt inverter of UPFC. The integral type regulator controls the internal voltage magnitude, E_{in}, in (2). The differential equation of E_{in} can be derived as follows,

$$\dot{E}_{in} = -K_S\frac{Droop}{x_t}E_{in} - K_S S_{UP} \tag{15}$$

$$+K_S V_{REF} - K_S\left(1-\frac{Droop}{x_t}\right)V_1^f.$$

Fig. 4(b) shows the structure of the control system of the SSSC. The amplifier type controller regulates the voltage magnitude, V_q, in (3). The differential equation can be derived as follows,

$$\dot{V}_q = -\frac{1}{\tau_F}V_q + \frac{K_F\left(P_{REF}+S_{UP}\right)}{V_1^f \tau_F} - \frac{K_F}{\tau_F} \tag{16}$$

$\mathbf{I_P^f}$ in (16) can be derived from the current through the series impedance, x_S, in Fig. 2(a). It indicates the real component of the current measured from the reference located at the phase angle of the voltage on the node 1 in Fig. 2(a). Thus, the measured current has the same phase angle with the complex power flow, and $\mathbf{I_P^f}$ implies the current component which contributes to the active and the reactive power flows, respectively. It can be derived as follows,

$$I_P^f = \frac{V_q}{x_S}\sin\left(\theta_q - \theta_1^f\right) + \frac{V_2^f}{x_S}\sin\left(\theta_1^f - \theta_2^f\right). \tag{17}$$

Fig. 4(c) is the structure of the control system of the series inverter of UPFC. It is assumed that the series injected voltage, $\mathbf{V_S}$, is composed of the component, V_P, which controls the active power flow and

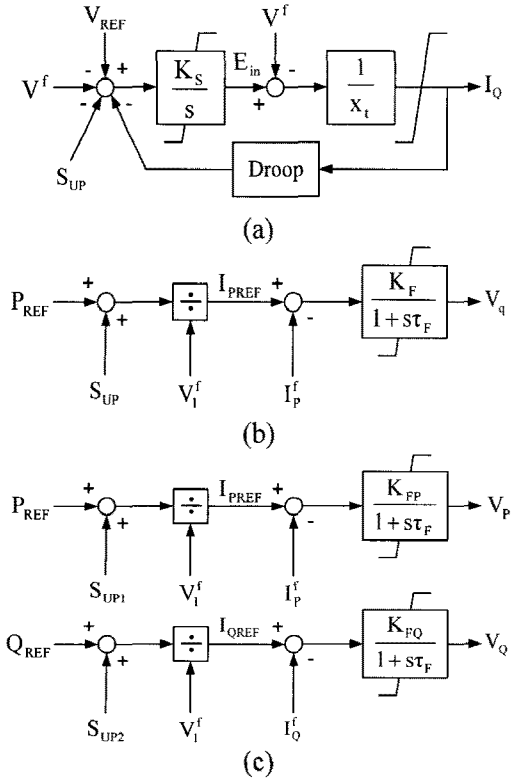

Fig. 4. The control system of (a) STATCOM, (b) SSSC, and (c) the series part of UPFC.

quadrature-phase component, V_Q, which control the reactive power flow in transmission line. Their differential equations can be derived as follows,

$$\dot{V}_P = -\frac{1}{\tau_F}V_P + \frac{K_{FP}\left(P_{REF}-S_{UP1}\right)}{V_1^f \tau_F} - \frac{K_{FP}}{\tau_F}I_P^f, \tag{18}$$

$$\dot{V}_Q = -\frac{1}{\tau_F}V_Q + \frac{K_{FQ}\left(Q_{REF}-S_{UP2}\right)}{V_1^f \tau_F} - \frac{K_{FQ}}{\tau_F}I_Q^f. \tag{19}$$

$\mathbf{I_P^f}$ and $\mathbf{I_Q^f}$ in (18) and (19) can be derived from the current through the series impedance, x_S, in Fig. 3(a). They indicate the real and the imaginary components of the current measured from the reference located at the phase angle of the voltage on the shunt inverter side node, which is the node 1 in Fig. 3(a). Thus, the measured current has the same phase angle with the complex power flow, and $\mathbf{I_P^f}$ and $\mathbf{I_Q^f}$ imply the current components which contribute to the active and the reactive power flows, respectively. They can be derived as follows,

$$I_P^f = \frac{V_S}{x_S}\sin\theta_S + \frac{V_2^f}{x_S}\sin\left(\theta_1^f - \theta_2^f\right), \tag{20}$$

$$I_Q^f = \frac{V_1^f}{x_S} + \frac{V_S}{x_S}\cos\theta_S - \frac{V_2^f}{x_S}\cos\left(\theta_1^f - \theta_2^f\right). \tag{21}$$

In (20) and (21), $V_S\sin\theta_S$ and $V_S\cos\theta_S$ are the components of the series injected voltage, $\mathbf{V_S}$. Since $V_S\sin\theta_S$ and $V_S\cos\theta_S$ contribute to the active and the reactive power flow components, they imply V_P and V_Q in Fig 4(c), respectively. Therefore, the series injected voltage, $\mathbf{V_S}$, is derived as follows,

$$\mathbf{V_S} = V_S\left(\cos\theta_S + j\sin\theta_S\right) = V_Q + jV_P, \tag{22}$$

$$\theta_S = \tan^{-1}\frac{V_P}{V_Q}. \tag{23}$$

According to (22), the equations (20), (21), and the active power supplied by the series inverter in (10) can be re-written as follows,

$$I_P^f = \frac{V_P}{x_S} + \frac{V_2^f}{x_S}\sin\left(\theta_1^f - \theta_2^f\right), \tag{24}$$

$$I_Q^f = \frac{V_1^f}{x_S} + \frac{V_Q}{x_S} - \frac{V_2^f}{x_S}\cos\left(\theta_1^f - \theta_2^f\right), \tag{25}$$

$$P^f = -\frac{V_1^f V_P}{x_S} + \frac{V_2^f V_P}{x_S}\cos\left(\theta_1^f - \theta_2^f\right) + \frac{V_2^f V_Q}{x_S}\sin\left(\theta_1^f - \theta_2^f\right). \tag{26}$$

As mentioned in (8), it is assumed that the shunt inverter of UPFC is the same as STATCOM. Thus, the control system of STATCOM is used for the shunt inverter of UPFC, except that the subscript sh is being used instead of Q in Fig. 4(a).

3.2. Damping controller modeling

A lead-lag type compensator is considered as a damping controller. As a supplementary input signal, the active power flow on the external node of FACTS is considered as in [12].

$$S_{UP} = K_W \frac{s\tau_W}{1+s\tau_W}\frac{1+s\tau_1}{1+s\tau_2}P_{flow}. \tag{27}$$

The differential equations of the state variables in (27) can be derived as follows,

$$\dot{x}_{SUP1} = -\frac{1}{\tau_W}x_{SUP1} + \frac{K_W}{\tau_W}P_{flow}, \tag{28}$$

$$\begin{aligned}\dot{x}_{SUP2} = &-\frac{1}{\tau_2}\left(1-\frac{\tau_1}{\tau_2}\right)x_{SUP1} - \frac{1}{\tau_2}x_{SUP2} \\ &+\frac{K_W}{\tau_2}\left(1-\frac{\tau_1}{\tau_2}\right)P_{flow},\end{aligned} \tag{29}$$

where x_{SUP1} and x_{SUP2} are the state variables of the wash-out and the lead-lag in (27), respectively. Equation (27) can be re-written using the state variables, x_{SUP1} and x_{SUP2}, as follows,

$$S_{UP} = -\frac{\tau_1}{\tau_2}x_{SUP1} + x_{SUP2} + \frac{K_W\tau_1}{\tau_2}P_{flow}. \tag{30}$$

Substituting (33) into (15), (16), (18), and (19) gives the differential equation of FACTS controllers equipped with the damping controller.

3.3. Algebraic equations

By the installation of FACTS controller, (13) and (14) can be re-written as follows,

$$\dot{\mathbf{x}}_{\mathbf{A}} = \mathbf{f}_{\mathbf{A}}(\mathbf{x}_{\mathbf{A}}, \mathbf{V}_{\mathbf{A}}), \tag{31}$$

$$\begin{aligned}\mathbf{F}_{\mathbf{A}} &= \begin{bmatrix}\mathbf{I(V)} \\ \mathbf{I}^{\mathbf{f}}(\mathbf{V}^{\mathbf{f}})\end{bmatrix} - \begin{bmatrix}\mathbf{Y} & \mathbf{Y}^{\mathbf{m}} \\ \mathbf{Y}^{\mathbf{n}} & \mathbf{Y}^{\mathbf{f}}\end{bmatrix}\begin{bmatrix}\mathbf{V} \\ \mathbf{V}^{\mathbf{f}}\end{bmatrix} \\ &= \mathbf{I}_{\mathbf{A}}(\mathbf{V}_{\mathbf{A}}) - \mathbf{Y}_{\mathbf{A}}\mathbf{V}_{\mathbf{A}} = \mathbf{0},\end{aligned} \tag{32}$$

where the subscript A implies the augmented quantities due to the FACTS controller and superscript f indicates the variables related to FACTS controller. $\mathbf{Y}^{\mathbf{m}}$, $\mathbf{Y}^{\mathbf{n}}$, and $\mathbf{Y}^{\mathbf{f}}$ are the admittance matrices augmented by FACTS installation. The detail expressions are described in [11].

The equation (32) can be decomposed into two parts as follows,

$$\mathbf{F} = \mathbf{I(V)} - \mathbf{YV} - \mathbf{Y}^{\mathbf{m}}\mathbf{V}^{\mathbf{f}} = \mathbf{0}, \tag{33}$$

$$\mathbf{F}^{\mathbf{f}} = \mathbf{I}^{\mathbf{f}}(\mathbf{V}^{\mathbf{f}}) - \mathbf{Y}^{\mathbf{n}}\mathbf{V} - \mathbf{Y}^{\mathbf{f}}\mathbf{V}^{\mathbf{f}} = \mathbf{0}. \tag{34}$$

The equivalent currents injected by FACTS controllers, $\mathbf{I}^{\mathbf{f}}(\mathbf{V}^{\mathbf{f}})$ in equations (34), can be expressed in 1- or 2-dimensional complex matrices as follows,

$$\mathbf{I}^{\mathbf{f}}_{\mathbf{STATCOM}}(\mathbf{x}, \mathbf{V}^{\mathbf{f}}) = \begin{bmatrix}\mathbf{I_Q}\end{bmatrix}, \tag{35}$$

$$\mathbf{I}^{\mathbf{f}}_{\mathbf{SSSC}}(\mathbf{x}, \mathbf{V}^{\mathbf{f}}) = \begin{bmatrix}-\mathbf{I_q} \\ \mathbf{I_q}\end{bmatrix}, \tag{36}$$

$$\mathbf{I}^{\mathbf{f}}_{\mathbf{UPFC}}(\mathbf{x}, \mathbf{V}^{\mathbf{f}}) = \begin{bmatrix}\mathbf{I_{sh}} + \mathbf{I_P} - \mathbf{I_S} \\ \mathbf{I_S}\end{bmatrix}, \tag{37}$$

where the 1st and 2nd rows in (36) and (37) correspond to the node 1 and 2 in Fig 2(b) and 3(b), respectively. The detailed expressions of the current elements in (35), (36), and (37) are described in (1)~(12).

4. LINEAR ANALYSIS

The linear analysis for small-signal stability studies is the most general method to estimate the dynamic stability of power system quantitatively. In this paper, the method is considered to get the parameters of FACTS controllers and damping controllers for dynamic stability enhancement.

Taking partial derivatives of (31) and (32) gives the linearized dynamic system equations as follows,

$$\Delta\dot{\mathbf{x}}_{\mathbf{A}} = \frac{\partial \mathbf{f}_{\mathbf{A}}}{\partial \mathbf{x}_{\mathbf{A}}}\Delta\mathbf{x}_{\mathbf{A}} + \frac{\partial \mathbf{f}_{\mathbf{A}}}{\partial \mathbf{V}_{\mathbf{A}}}\Delta\mathbf{V}_{\mathbf{A}}, \tag{38}$$

$$\frac{\partial \mathbf{F}_{\mathbf{A}}}{\partial \mathbf{x}_{\mathbf{A}}}\Delta\mathbf{x}_{\mathbf{A}} + \frac{\partial \mathbf{F}_{\mathbf{A}}}{\partial \mathbf{V}_{\mathbf{A}}}\Delta\mathbf{V}_{\mathbf{A}} = \mathbf{0}. \tag{39}$$

Substituting (39) into (38), the state space matrix for eigen-value analysis can be derived as follows,

$$\Delta\dot{\mathbf{x}}_{\mathbf{A}} = \left[\frac{\partial \mathbf{f}_{\mathbf{A}}}{\partial \mathbf{x}_{\mathbf{A}}} - \frac{\partial \mathbf{f}_{\mathbf{A}}}{\partial \mathbf{V}_{\mathbf{A}}}\left[\frac{\partial \mathbf{F}_{\mathbf{A}}}{\partial \mathbf{V}_{\mathbf{A}}}\right]^{-1}\frac{\partial \mathbf{F}_{\mathbf{A}}}{\partial \mathbf{x}_{\mathbf{A}}}\right]\Delta\mathbf{x}_{\mathbf{A}} = \mathbf{A}\Delta x_{\mathbf{A}}. \tag{40}$$

A set of linearized differential equations for each FACTS controller in equation (38) can be derived from the equations (15)-(19), and (24)-(25). Since STATCOM has one state variable, E_{in}, taking partial derivatives of equation (15) gives the 1-dimensional linearied differential equation. SSSC has one state variable, V_q. Substituting equation (17) into equation (16) and then taking partial derivatives of equation (16), the 1-dimensional linearized differential equation is derived. UPFC has three state variables, V_P, V_Q, and E_{in}. Substituting equations (24) and (25) into (18) and (19) and taking partial derivatives of

(16), (18), and (19), the 3-dimensional linearized differential equation is derived. If the damping controller in (27) is equipped on FACTS controller, the 2 differential equations of damping controller are added to the linearized differential equations of each FACTS controller.

In order to get the linearized algebraic equations for each FACTS controller, (32) may be decomposed into the real and the imaginary parts. In the case of STATCOM, it becomes a 2-dimensional algebraic equation as follow,

$$\begin{bmatrix} F_R^f \\ F_I^f \end{bmatrix} = \begin{bmatrix} I_{QR} \\ I_{QI} \end{bmatrix} + \sum_{i=1}^{n} \begin{bmatrix} -Y_{1i}^n V_i \cos\left(\phi_{1i}^n + \theta_i\right) \\ -Y_{1i}^n V_i \cos\left(\phi_{1i}^n + \theta_i\right) \end{bmatrix} + \begin{bmatrix} -Y_{11}^f V^f \cos\left(\phi_{11}^n + \theta^f\right) \\ -Y_{11}^f V^f \sin\left(\phi_{11}^n + \theta^f\right) \end{bmatrix} = \mathbf{0}. \tag{41}$$

In the case of SSSC and UPFC, it becomes 4-dimensional algebraic equations as follows,

$$\begin{bmatrix} F_{R1}^f \\ F_{I1}^f \\ F_{R2}^f \\ F_{I2}^f \end{bmatrix} = \begin{bmatrix} -I_{qR} \\ -I_{qI} \\ I_{qR} \\ I_{qI} \end{bmatrix} + \sum_{i=1}^{n} \boldsymbol{\alpha}_\mathbf{i} + \sum_{k=1}^{2} \boldsymbol{\beta}_\mathbf{k} = \mathbf{0}, \tag{42}$$

$$\begin{bmatrix} F_{R1}^f \\ F_{I1}^f \\ F_{R2}^f \\ F_{I2}^f \end{bmatrix} = \begin{bmatrix} I_{shR} + I_{PR} - I_{SR} \\ I_{shI} + I_{PI} - I_{SI} \\ I_{SR} \\ I_{SI} \end{bmatrix} + \sum_{i=1}^{n} \boldsymbol{\alpha}_\mathbf{i} + \sum_{k=1}^{2} \boldsymbol{\beta}_\mathbf{k} = \mathbf{0},$$

$$\boldsymbol{\alpha}_\mathbf{i} = \begin{bmatrix} -Y_{1i}^n V_i \cos\left(\phi_{1i}^n + \theta_i\right) \\ -Y_{1i}^n V_i \sin\left(\phi_{1i}^n + \theta_i\right) \\ -Y_{2i}^n V_i \cos\left(\phi_{2i}^n + \theta_i\right) \\ -Y_{2i}^n V_i \sin\left(\phi_{2i}^n + \theta_i\right) \end{bmatrix},$$

$$\boldsymbol{\beta}_\mathbf{k} = \begin{bmatrix} -Y_{1k}^f V_k^f \cos\left(\phi_{1k}^f + \theta_k^f\right) \\ -Y_{1k}^f V_k^f \sin\left(\phi_{1k}^f + \theta_k^f\right) \\ -Y_{2k}^f V_k^f \cos\left(\phi_{2k}^f + \theta_k^f\right) \\ -Y_{2k}^f V_k^f \sin\left(\phi_{2k}^f + \theta_k^f\right) \end{bmatrix}, \tag{43}$$

where R and I indicate real and imaginary parts, respectively, and Ys and Φs correspond to the magnitudes and the phase angles of the elements of admittance matrices having the same super- and sub-scripts in (32).

Then, taking partial derivatives of (41), (42), and (43) gives sets of linearized algebraic equations for each FACTS controller in (39).

5. NONLINEAR ANALYSIS

The partial derivatives with respects to the voltage magnitudes and the phase angles, $\partial \mathbf{F}_A / \partial \mathbf{V}_A$, can be used as Jacobian matrix, $\mathbf{J}_A$, for the Newton iteration method in time-domain simulations as described in [11].

$$\begin{bmatrix} \Delta \mathbf{F_R} \\ \Delta \mathbf{F_I} \\ \Delta \mathbf{F_R^f} \\ \Delta \mathbf{F_I^f} \end{bmatrix} = \begin{bmatrix} \mathbf{J} & \mathbf{J^m} \\ \mathbf{J^n} & \mathbf{J^f} \end{bmatrix} \begin{bmatrix} \Delta \mathbf{V} \\ \Delta \boldsymbol{\theta} \\ \Delta \mathbf{V^f} \\ \Delta \boldsymbol{\theta}^\mathbf{f} \end{bmatrix} \tag{44}$$

In the time-domain simulation algorithm, (31) is used to update the state variable, $\mathbf{x}$, and then the algebraic variables in (32) are solved by the Newton formula at every time step. The detail expressions are described in [11].

6. CASE STUDIES

6.1. A sample power system model

A sample system used in the case study is a two-area power system model shown in Fig. 5 [13]. It is assumed that all generators are the 4th order 2-axis models equipped with the 1st order fast exciters. The equations of 2-axis model and the fast exciters are described in [14] and [13], respectively. All loads are assumed to be the constant impedance type. All machine and system parameters are listed in Appendix. It is assumed that the FACTS controllers which have the rating of 100MVA are installed in the middle of the tie lines.

The system has one inter-area mode with very poor damping. The parameters of each FACTS controller in Fig. 4 and the damping controller in (27) are estimated to increase the damping ratio of inter-area oscillations using the linear analysis and its effect is then verified by the time-domain simulation. The linear analysis and time-domain simulations algorithms are programmed by MATLAB m-file code in 60Hz frequency base. Since the inverters have very fast operating speed in several tens of milliseconds, the time constant, τ_F, is considered within $0.01 \le \tau_F \le 0.05$

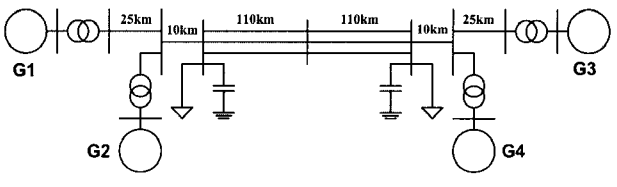

Fig. 5. A sample 2-area power system.

seconds. It is assumed that all of the voltage and currents injected by FACTS controllers are zero in initial condition.

6.2. Linear analysis

6.2.1 Without damping controller

Fig. 6 show the eigen-value locus of the inter-area oscillations in the case of SSSC installed within $0.0 \leq K_F \leq 1.0$. As K_F is increased, the frequency of the mode is decreased. The damping ratios are reached to the maximum values, and then decreased for a higher value. In Fig. 6, the denoted point on each curve indicates the point having the maximum damping ratio for each time constant. They are listed in Table 1.

Since STATCOM is the reactive power compensator for voltage regulation, it has little effect on the inter-area oscillation. Therefore, the linear analysis for STATCOM without damping controller is omitted. Its integrated parameter, K_S in Fig. 4(a), is assumed to be 20.0 which is enough high to regulate the voltage. The value is also applied to the shunt inverter of UPFC.

In the case of UPFC being installed, the eigen-value locus of inter-area oscillations is shown in Fig. 7. The gains, K_{FP} and K_{FQ}, have the range, $0.0 \leq K_{FP}, K_{FQ} \leq 1.0$. As K_{FP} and K_{FQ} are increased, the damping ratios

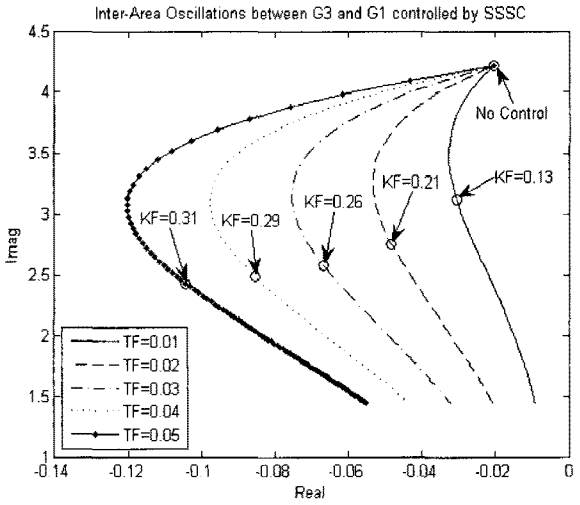

Fig. 6. Eigen-value locus of the inter-area oscillation mode controlled by SSSC.

Table 1. The linear analysis results for SSSC.

K_F	τ_F	Eigen-Value (λ)		Damp. ratio (ζ)	Freq. (Hz)
		Real (σ)	Imag. (ω)		
K_F = 0.0		-0.0203	4.2177	0.0048	0.6713
0.13	0.01	-0.0305	3.1281	0.0097	0.4979
0.21	0.02	-0.0483	2.7587	0.0175	0.4391
0.26	0.03	-0.0667	2.5815	0.0258	0.4109
0.29	0.04	-0.0855	2.4893	0.0343	0.3962
0.31	0.05	-0.1044	2.4327	0.0429	0.3872

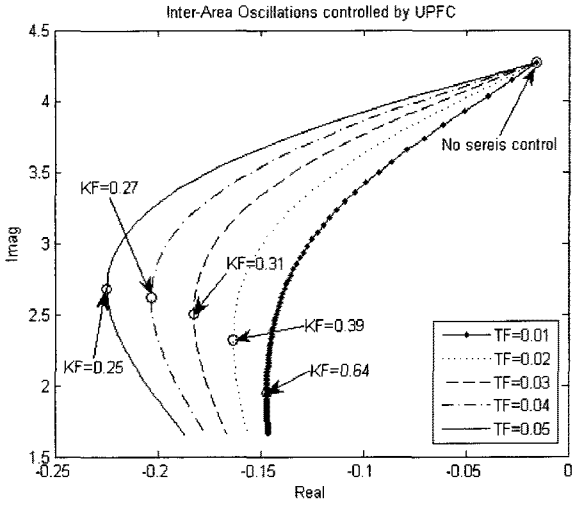

Fig. 7. Eigen-value locus of the inter-area oscillation mode controlled by UPFC.

Table 2. The linear analysis results for UPFC.

K_{FP}, K_{FQ}	τ_F	Eigen-Values (λ)		Damp. ratio (ζ)	Freq. (Hz)
		Real (σ)	Imag. (ω)		
K_{FP},K_{FQ}=0.0		-0.0160	4.2640	0.0037	0.6786
0.64	0.01	-0.1469	1.9545	0.0750	0.3111
0.39	0.02	-0.1633	2.3243	0.0701	0.3699
0.31	0.03	-0.1826	2.5061	0.0727	0.3989
0.27	0.04	-0.2032	2.6174	0.0774	0.4166
0.25	0.05	-0.2247	2.6804	0.0836	0.4266

of inter-area oscillations are increased. However, since the incremental ratio of damping is decreased and the frequency is excessively low in the high values of gains, they are set on the point having the minimum real part of eigen-values. The denoted point on each curve has the minimum real part of eigen-values. They are summarized in Table 2.

6.2.2 With damping controller

As described above, the STATCOM has little effect on the inter-area oscillation. The SSSC and UPFC have a limit to increase the damping ratio. Therefore, the supplementary controller in (35) is considered to enhance the performance of FACTS controllers. Since the FACTS controller is assumed to be installed in the middle of tie lines in Fig. 5, the input, P_{flow}, is set to the active power flow in the tie lines. The time constants in (27) are computed from the phase lead-lag angle based on the formula described in [13]. The phase lead angle is considered in every 15° within ±30°. The wash-out time constant is set to 5.0 second.

Fig. 8 shows the locus of inter-area oscillations mode controlled by STATCOM and SSSC with damping controller. The gain, K_W, has the range, $0.0 \leq K_W \leq 1.0$. In the case of the damping controller equipped in SSSC, the higher K_W makes the higher

damping ratio. However, the damping controller equipped in STATCOM has a limit to increase damping ratio. Each eigen-value having the maximum damping ratio is listed in Tables 3 and 4, and the time constants, τ_1 and τ_2, for each compensation angle are listed in Table 5.

As described in Tables 3 and 4, the most effective compensation angles for STATCOM and SSSC are 30° lag and 15° lead, respectively. Those show the difference of dynamic characteristics between STATCOM and SSSC. Comparing STATCOM and SSSC, it can be confirmed that SSSC is more effective than STATCOM. The result indicates that the series type FACTS controller is more profitable to damp inter-area low frequency oscillations.

Different from STATCOM and SSSC, UPFC is composed of the series and the shunt inverters. Additionally, since the series inverter control system is modeled with the real and the reactive parts, as shown in Fig. 4, the three supplementary controllers can be equipped in UPFC. Fig. 9 shows the locus of inter-area modes controlled by UPFC with damping controllers on each inverter control system. In Table 8, the results are described in detail.

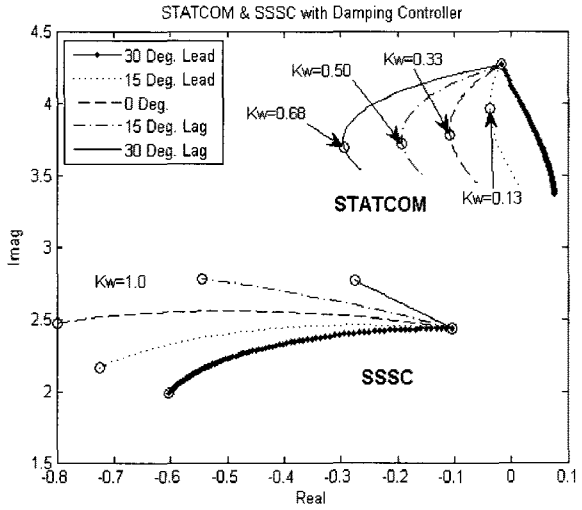

Fig. 8. Eigen-value locus controlled by STATCOM and SSSC with damping controller.

Table 3. The linear analysis results for STATCOM with damping controller.

Lead angle	K_W	Eigen-Value (λ)		Damp. ratio (ζ)	Freq. (Hz)
		Real (σ)	Imag. (ω)		
K_W= 0.0		-0.0160	4.2640	0.0037	0.6786
30°	0.0	-0.0160	4.2640	0.0037	0.6786
15°	0.13	-0.0372	3.9624	0.0094	0.6306
0°	0.33	-0.1071	3.7781	0.0283	0.6013
-15°	0.50	-0.1921	3.7150	0.0516	0.5913
-30°	0.68	-0.2937	3.6867	0.0794	0.5868

As shown in Fig. 9 and Table 6, the positive gain with 15° lead-angle of the damping controller is the most effective for the active power flow control system in the series inverter of UPFC. On the other hand, the negative grain in 30° lead-angle is the most effective in the reactive power flow control system and the shunt inverter control systems. The time constants for each compensation angle and each controlled part are listed in Table 7.

Comparing the UPFC with the SSSC, the effect of damping controller equipped in the active power control system of the series inverter of UPFC is much more effective than the controller equipped in the SSSC. It is because the SSSC can control the active

Table 4. The linear analysis results for SSSC with damping controller.

Lead angle	K_W	Eigen-Value (λ)		Damp. Ratio (ζ)	Freq. (Hz)
		Real (σ)	Imag. (ω)		
K_W = 0.0		-0.1044	2.4327	0.0429	0.3872
30°	1.0	-0.6029	1.9855	0.2906	0.3160
15°	1.0	-0.7249	2.1594	0.3183	0.3437
0°	1.0	-0.7997	2.4710	0.3079	0.3933
-15°	1.0	-0.5441	2.7774	0.1922	0.4420
-30°	1.0	-0.2752	2.7643	0.0991	0.4400

Table 5. The time constants for lead-lag blocks.

Lead angle	STATCOM		SSSC	
	τ_1	τ_2	τ_1	τ_2
30°	0.4062	0.1354	0.7120	0.2373
15°	0.3056	0.1800	0.5357	0.3154
0°	0.2345	0.2345	0.4111	0.4111
-15°	0.1800	0.3056	0.3154	0.5357
-30°	0.1354	0.4062	0.2373	0.7120

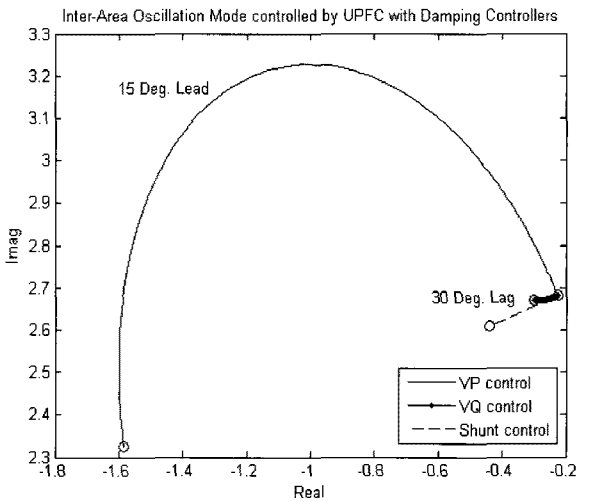

Fig. 9. Eigen-value locus controlled by UPFC with damping controller.

Table 6. The linear analysis results for UPFC with damping controller.

S_{UP}	Lead angle	Eigen-Value (λ)		Damp. (ζ)	Freq. (Hz)
		Real (σ)	Imag. (ω)		
K_W = 0.0		-0.2247	2.6804	0.0836	0.4266
V_P	15°	-1.5850	2.3236	0.5635	0.3698
V_Q	30°	-0.3013	2.6696	0.1122	0.4249
E_{in}	30°	-0.4424	2.6079	0.1672	0.4151

Table 7. The parameters for the damping controller in UPFC.

S_{UP}	Lead angle	K_W	τ_1	τ_2
V_P	15°	1.0	0.4862	0.2863
V_Q	30°	-1.0	0.6462	0.2154
E_{in}	30°	-1.0	0.6462	0.2154

power flow indirectly, by compensating the reactive power, but the series inverter of UPFC can supply the active power and control the active power flow directly. Contrarily, the damping controller equipped in the reactive power control system of the series part of UPFC is less effective than the SSSC. It is because the SSSC is designed to control the active power flow, but the reactive power flow control system is modeled to control the reactive power.

Comparing with the STATCOM, the effect of damping controller equipped in the shunt inverter control system is more effective than the controller equipped in the STATCOM. Additionally, the phase angles for compensation and the gain are also different. It shows that the dynamic characteristic difference between the STATCOM and UPFC.

6.3. Time-domain simulations

To verify the results described above, the time-domain simulations are performed for each system having different FACTS controllers with or without damping controllers. The 3 phase fault is applied to the load bus in area 1 shown in Fig. 5 at 0.5 second, and then it is cleared after 6 cycles. The simulations are continued for 10 seconds. The modified Euler method is used for numerical integration, and the integration time step is 0.5 cycle.

6.3.1 STATCOM

Fig. 10 shows the time domain simulation results for the STATCOM. The limits in Fig. 4(a) are $0.8 \leq E_{in} \leq 1.2$, $-1.25 \leq I_Q \leq 1.25$ in p.u. on 100MVA base. The parameters of STATCOM and damping controller correspond to the row for 30° lag compensation in Tables 3 and 5. The dotted, the dashed, and the solid lines indicate no FACTS, the without-, and the with-damping controller cases, respectively. As mentioned above, the STATCOM without damping controller has little effect on the inter-area oscillations. However, the

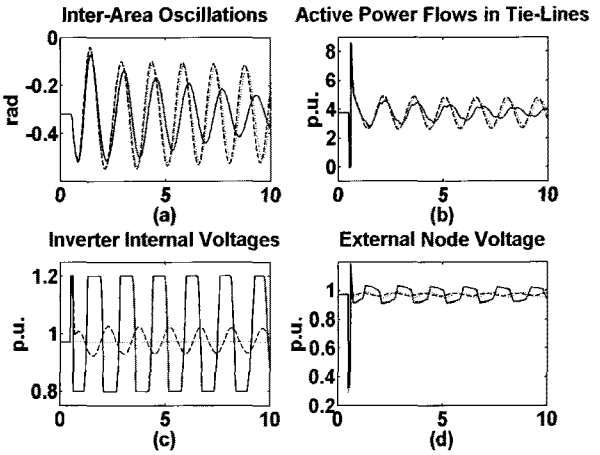

Fig. 10. (a) Inter-area oscillations, (b) active power flows on tie-lines, (c) internal voltage of STATCOM, E_{in}, (d) external node voltage, V^f.

STATCOM with damping controller can damp the inter-area oscillations and regulate the active power flow on tie-lines. They are evident in Fig. 10(a) and 10(b). However, since the inverter with damping controller disturbs the terminal voltage in order to control the active power flow in the tie lines, the STATCOM with damping controller has a negative effect on the external voltage, V^f. They are well shown in Figs. 10(c) and 10(d).

6.3.2 SSSC

Fig. 11 shows the time domain simulation results for SSSC. The limit in Fig. 4(a) is $-0.05 \leq V_q \leq 0.05$ in p.u. on 100MVA base. The parameters of SSSC are listed in the row for $\tau_F = 0.05$ in Table 1, and the parameters of damping controller are employed from the row for 15° lead compensation in Tables 4 and 5. The dotted, the dashed, and the solid lines indicate no FACTS, the without-, and the with-damping controller cases, respectively. As shown in Table 1, the SSSC

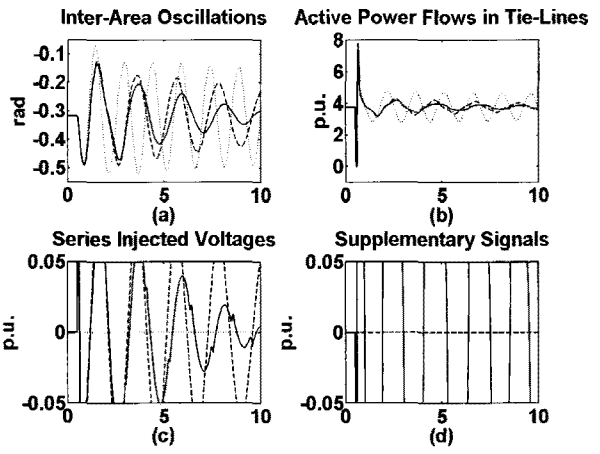

Fig. 11. (a) Inter-area oscillations, (b) Active power flows on tie-lines, (c) series injected voltage magnitudes, V_q, (d) damping controller output, S_{UP}.

without damping controller can increase the damping ratio from 0.0048 to 0.0429, and the damping controller can additionally increase the damping ratio up to 0.3183. The effects are shown on the inter-area oscillations and the active power flows in Fig. 11(a) and 11(b). The injected voltage magnitudes, V_q, by SSSC are shown in Fig. 11(c), and the supplementary signal of damping controller is shown in Fig. 11(d). It is confirmed that the damping controller prevents the SSSC oscillate excessively and help the compensation actions of SSSC.

6.3.3 UPFC

Figs. 12 and 13 show the time-domain simulation results for UPFC. The limits in Figs. 4(a) and 4(c) are $0.8 \le E_{in} \le 1.2$, $-1.25 \le I_{sh} \le 1.25$, $-0.05 \le V_P, V_Q \le 0.05$ in p.u. in 100MVA base. The parameters of the row for $\tau_F = 0.05$ in Table 2 are used for the simulation, and the parameters of damping controller are listed on the row for V_P control in Table 7. In Figs. 12 and 13, the dotted, the dashed, and the solid lines indicate the no FACTS controller, the without-, and the with-damping controller cases, respectively.

As shown in Fig. 12(a), the UPFC has a positive effect on the inter-area oscillation, and then the damping is increased by the damping controller and the oscillation is damped out. The active power flows in Fig. 12(b) shows the active power flow control effect of UPFC.

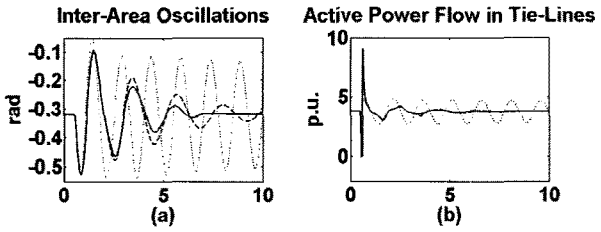

Fig. 12. (a) Inter-area oscillations, (b) active power flows on tie-lines.

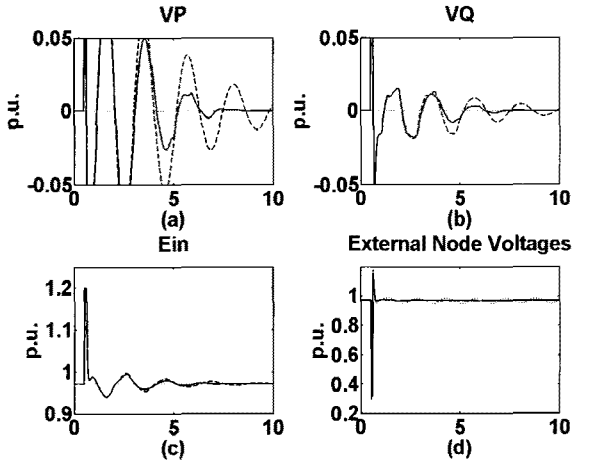

Fig. 13. The series injected voltages, (a) V_P and (b) V_Q, (c) internal voltage, E_{in}, and (d) shunt inverter side voltage, V_1^f.

Figs. 13(a) and 13(b) show the injected voltages by the series inverter of UPFC. The damping controller helps the series inverter to control the active power flow. Fig. 13(c) shows the voltage magnitude, E_{in}, generated by the shunt inverter of UPFC. It shows the voltage regulation actions of the shunt inverter in Fig. 13(d). The series injected voltage can make the voltage oscillations on the external nodes. However, as shown in Fig. 13(d), the external node voltage, V_1^f, in the shunt inverter side node is regulated by the shunt inverter. Figs. 13(b) and 13(d) show the simultaneous controllability.

Comparing the simulation results for each FACTS controller in linear analysis and time-domain simulation, the most effective controller for damping of inter-area oscillations is UPFC. The effect of SSSC is less than UPFC, and STATCOM has the least effects on the inter-area oscillations.

Among these FACTS controllers, the popular controllers are STATCOM and UPFC. Because STATCOM has the advantage of reactive power compensation, and UPFC has controllability for active and reactive power flow and voltage regulation. Consequently, many research results have been presented for STATCOM and UPFC. SSSC is relatively unnoticed, and there are not many research reports for SSSC. However, since it is more effective than Thyristor Controlled Series Compensator (TCSC) which is widely used, it may be able to substitute TCSC where the series compensation is needed without the voltage regulation.

7. CONCLUSIONS

This paper proposed a current injection model of FACTS controllers for power system dynamic stability studies. The method can be easily applied to the linear and the nonlinear analysis, and adopt any kind of FACTS controllers regardless of model types.

As described above, it can be applied to the linear and nonlinear analysis algorithm for power system dynamics studies. Using the linear analysis, the parameters of each FACTS controller are estimated in order to have a positive effect on the inter-area oscillation mode. And, the supplementary controller for damping control is designed to increase the damping ratio of power system. The results are verified by nonlinear analysis using time-domain simulations.

The results accomplished by the proposed methods show the differences among FACTS controllers and their control schemes for the inter-area oscillations in power system. According to the results, UPFC is the most effective FACTS controller for damping inter-area oscillations. And, SSSC is more effective than STATCOM. The analysis results show the

characteristics of each FACTS controller. It shows the effectiveness and actuality of the proposed model.

APPENDIX

Each step-up transformer has an impedance of $j0.15$ p.u. on 900MVA and a 20/230kV base. The nominal transmission system voltage was 230kV. The line length is as shown in Fig. 5. The parameters of the lines in p.u. on 100MVA and a 230kV bases are r = 0.0001 p.u./km, x_L = 0.001 p.u./km, and b_C = 0.00175 p.u./km.

Each generator has a rating of 100MVA and 20kV and the parameters in p.u. is as follows, H = 58.5(G1, G2), 55.58(G3, G4), D = 0.0, τ'_{d0} = 8.0, τ'_{q0} = 0.4, x_d = 0.2, x'_d = 0.033, x_q = 0.18, and x'_q = 0.033.

The FACTS controllers have a rating of 100MVA and the parameters in p.u. are as follows, x_S = 0.05, x_t = 0.1, and *Droop* = 0.0.

REFERENCES

[1] Y. H. Song and A. T. Johns, *Flexible AC Transmission Systems (FACTS)*, The Institution of Electrical Engineers, London, 1999.

[2] N. G. Hingorani and L. Gyugyi, *Understanding FACTS*, The Institute of Electrical and Electronics Engineers, New York, 2000.

[3] L. Gyugyi, "Dynamic compensation of AC transmission lines by solid-state synchronous voltage sources," *IEEE Trans. on Power Delivery*, vol. 9, no. 2, pp. 904-911, April 1994.

[4] L. Gyugyi, C. D. Schauder, S. L. Williams, T. R. Rietman, D. R. Torgerson, and A. Edris, "The unified power flow controller: A net approach to power transmission control," *IEEE Trans. on Power Delivery*, vol. 10, no. 2, pp. 1085-1097, April 1995.

[5] L. Gyugyi, "Static synchronous series compensator: A solid-state approach to the series compensation of transmission lines," *IEEE Trans. on Power Delivery*, vol. 12, no. 1, pp. 406-413, January 1997.

[6] M. Noroozian, L. Angquist, M. Ghandhari, and G. Andersson, "Improving power system dynamics by series-connected FACTS devices," *IEEE Trans. on Power Delivery*, vol. 12, no. 4, pp. 1635-1641, October 1997.

[7] H. F. Wang, "Phillips-Heffron model of power system installed with STATCOM and applications," *IEE Proc. of Generation, Transmission, Distribution*, vol. 146, no. 5, pp. 521-527, September 1999.

[8] H. F. Wang, "A unified model for the analysis of FACTS devices in damping power system oscillations - Part III: Unified power flow controller," *IEEE Trans. on Power Delivery*, vol. 15, no. 3, pp. 978-983, July 2000.

[9] H. Kim and S. Kwon, "The study of FACTS impacts for probabilistic transient stability," *J. of Electr. Eng. Technol.*, vol. 1, no. 2, pp. 129-136, June 2006.

[10] S. Kim, H. Song, B. Lee, and S. Kwon, "Enhancement of interface flow limit using static synchronous series compensators," *J. of Electr. Eng. Technol.*, vol. 1, no. 3, pp. 313-319, September 2006.

[11] K. M. Son and R. H. Lasseter, "A Newton-type current injection model of UPFC for studying low-frequency oscillations," *IEEE Trans. on Power Delivery*, vol. 19, no. 2, pp. 694-701, April 2004.

[12] Z. Huang, Y. Ni, C. M. Chen, F. F. Wu, S. Chen, and B. Zhang, "Application of unified power flow controller in interconnected power systems - modeling, interface, control strategy and case study," *IEEE Trans. on Power Systems*, vol. 15, no. 2, pp. 817-824, May 2000.

[13] P. Kundur, *Power System Stability and Control*, McGraw-Hill, New York, 1994.

[14] P. M. Anderson and A. A. Fouad, *Power System Control and Stability*, Institute of Electrical and Electronics Engineers, U.S.A., 2003.

Jungsoo Park received the B.S. and M.S. degrees in Electrical Engineering from Korea University in 2002 and 2004, respectively. Currently, he is a Ph.D. candidate student with the School of Electrical Engineering at Korea University. His research interests include power system dynamic stability and control, and FACTS controllers.

Gilsoo Jang received the B.S. and M.S. degrees in Electrical Engineering from Korea University in 1991 and 1994, and the Ph.D. degree in Electrical Engineering from Iowa State University in 1997. Currently, he is a Professor with the School of Electrical Engineering at Korea University. His research interests include power quality and power system control.

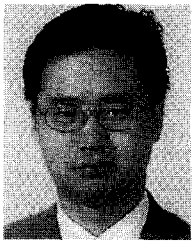

Kwang M. Son received the B.S., M.S., and Ph.D. degrees in Electrical Engineering from Seoul National University in 1989, 1991, and 1996, respectively. Currently, he is a Professor with the Department of Electrical Engineering at Dong-Eui University. His research interests include flexible AC transmission systems (FACTS) and distributed resources.